Investigation of the Stability of Cu/NbTi Multifilament Composite Wires

Frederic Trillaud, Frederic Ayela, Arnaud Devred and Pascal Tixador

***Abstract*— The thermo-electric stability of Cu/NbTi multifilament composite wires remains an important issue for magnet designers, especially, with respect to localized heat disturbances of short durations. Numerous attempts have been carried out to quantify the actual amount of energy needed to trigger a quench in superconductors. Various technologies are available to simulate quench precursors, but they are not fully satisfactory in terms of reproducibility and accuracy of the measurements. In the present paper, we report the results obtained with a novel heating method based on a fibered diode laser.**

***Index Terms*— optical absorption, quench energy, quench propagation velocity, single-mode diode laser, superconducting wires.**

I. Introduction

WHILE pushing the technology of superconducting magnets to reach the highest possible magnetic fields, magnet designers must take into account two requirements: reliability and safety. Indeed, by working at the edge of transport-current capacity of low temperature superconductors, any small energetic disturbance may result in a sudden conversion of the entire stored magnetic energy into heat dissipation. A potentially damageable situation for the operator and/or the electric and mechanical integrity of the magnet.

Numerous studies have been carried out to relate the unpredictable behavior of high current density magnets to mechanical disturbances occurring within its winding. Many years of experience point out disturbances of small spatial extensions and short durations as the most likely quench precursors [1], [2]. Various heater technologies have been developed to simulate the ensuing heat disturbances at the quench origins [3]-[5]. However, because of the difficulties to develop reliable and calibrated heaters, the search is still going on.

At CEA/Saclay, we have been working on a new heater technology based on commercial diode lasers. Two previous papers have been dedicated to the description and the preliminary results obtained with this technology [6], [7]. Hereinafter, we briefly detail new improvements implemented on the experimental setup. We also discuss measurement results and a preliminary numerical analysis.

Manuscript received October 5, 2005. This work is partly supported by Alstom/MSA and was mainly carried out at CEA/Saclay.

F. Trillaud is with CEA/Saclay, DSM/DAPNIA/SACM, 91191 Gif-Sur-Yvette cedex, France (phone: (+33) 1 69 08 61 79 and email: trillaud@dapnia.cea.fr).

F. Ayela is with CNRS-CRTBT, 38000 Grenoble cedex, France.

A. Devred is with CEA/Saclay, DSM/DAPNIA/SACM, and CERN/AT/MAS, CH-1211, Geneva 23, Switzerland.

P. Tixador is with CNRS-CRTBT, 38000 Grenoble cedex, France.

TABLE I
Salient Parameters of Laser Heater and Calibration Diode.

	Laser heater 293 K	Calibration diode 288 K
Max DC output power (W)	1.35	$\geq$0.3
Maximum current (A)	2	$\geq$0.9
Threshold current (A)	0.289	$\sim$0.19
Peak wavelength (nm)	807.4 $\pm$10	840

II. Experimental Setup

A. Laser Heater

a) Diode Laser and Optical Fibers: We rely on a commercial diode laser delivering a maximum optical power of $\sim$1.35 W whose salient parameters are listed in Table I. The diode laser is implemented on top of the cryostat and is operated at 293 K. To ensure the stability of the optical output power, its temperature is controlled by a Peltier element attached to it.

To transmit the light beam to the sample, the diode laser is pre-coupled to a standard $\sim$20-cm-long optical fiber, which is extended by an additional $\sim$1.7-m-long fiber. The tip of the optical fiber extension has been customized to ensure by a proper positioning that the entire cone of light flowing out of the fiber strikes the wire sample surface.

b) Optical Power Transmission Losses: A few tests have been carried out to estimate the transmission losses for our specific application. We study the influence of various parameters such as: 1) interconnection of optical fibers, 2) cryogenic environment and 3) thermal cycling. For these tests, the temperature of the diode laser was regulated at 293 K and we recorded its DC optical power output versus forward current characteristic.

Figure 1 shows a few results. The connector between fiber extension and pre-coupled fiber is the main source of transmission losses, estimated to $\sim$16%. The presence of the cryogenic coolant (simulated by dipping 2/3 of the fiber into LN_2) induced additional losses of $\sim$5%. No influence of the thermal cycling could be unveiled from our tests.

To estimate the energy pulse flowing from the tip of the optical fiber extension, we fitted the test data for which 2/3 of the fiber was wetted by LN_2 (no further degradation was assumed from 77 K to 4.2 K). Knowing the parameters of the current pulse supplied to the diode laser, we can then derive the pulse energy.

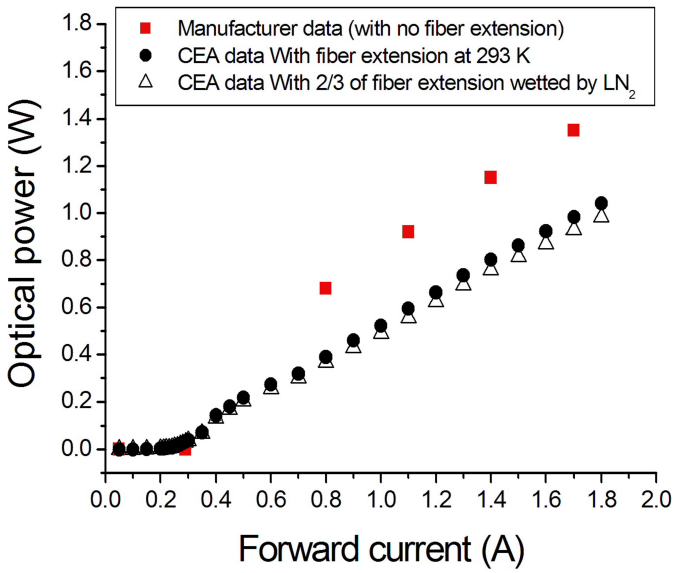

Fig. 1. DC optical power versus forward current characteristic of diode laser used in stability experiment at CEA/Saclay.

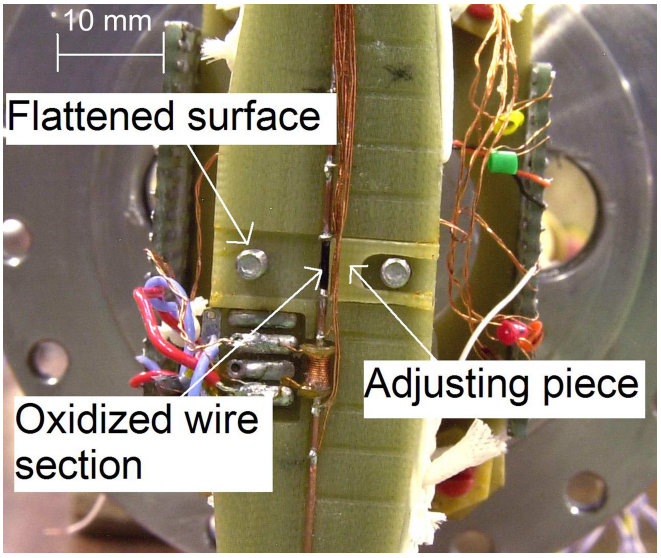

Fig. 2. Bottom view of machined sample holder and of fixtures to position and maintain wire sample into its V-shaped groove.

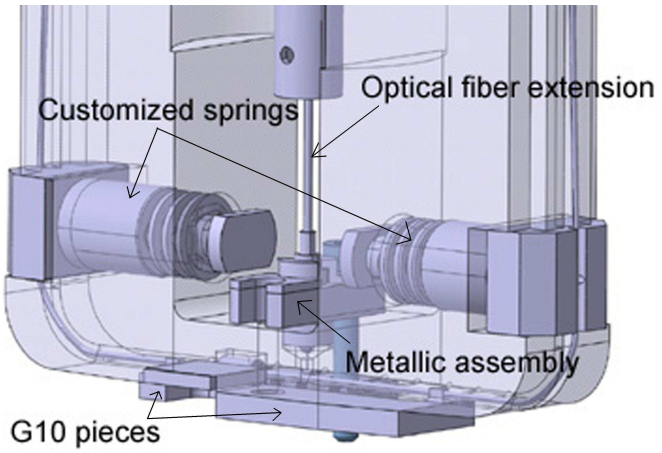

Fig. 3. 3D view of sample holder featuring clamping devices to position the tip of fiber extension and to maintain wire sample into its lodging.

B. Oxidation of Cu/NbTi Multifilament Composite Wire

To carry out stability tests, we used a bare LHC-02-type Cu/NbTi multifilament composite wire supplied by Alstom/MSA. In view of our preliminary tests on bare samples [6], it appeared necessary to increase the sample optical absorption in the near-infrared to benefit from the full power of the diode laser. Therefore, a low-temperature oxidation process was applied to blacken the sample surface and form a thin layer of cupric and cuprous oxides [8]. The excess oxidation was chemically etched so as to leave only a ∼3-mm-long blackened section at the center of the sample (see Fig. 2).

C. Stability Probe and Sample Holder

The probe for stability tests has been designed to carry out measurements in pool boiling helium I at 4.2 K and in a background magnetic flux density of up to 7 T. The diode laser is mounted at the top of the probe and the optical fiber extension runs to its bottom where the sample sits [7].

Figure 2 shows a bottom view of the sample holder. Two flattened surfaces have been filed near its center. They house two adjusting pieces, which help maintaining the oxidized portion of the wire in front the optical fiber tip. As depicted in Figure 3, additional customized springs help tensioning the sample while two G10 pieces limit its displacement during cold tests. To ensure that all the light strikes the wire sample surface, a special metallic assembly clamps the tip of the optical fiber extension to the the sample holder.

Three pairs of voltage taps with two common taps are soldered to the sample. Voltage drop, V_1, which covers a distance of ∼6 mm, encompasses the heated zone, and monitors the early evolution of normal zones. The remaining voltage drops, further down the sample, enable to assess Normal Zone Propagation Velocities.

III. Calibration "Proof-Test"

A calibration test has been performed to estimate the actual amount of energy absorbed by the wire sample. This test was originally planned to be carried out *in situ*, with the same experimental setup as for the stability tests. Unfortunately, sealing issues, that could not be solved in the time frame of this work, prevented us from doing it at CEA/Saclay and forced us to rely on a different experimental setup housed at CNRS/CRTBT (Grenoble, France) with a different diode laser [9]. Salient parameters of the calibration diode laser are listed in Table I.

Calibration tests are based on a bolometric technology illustrated in Figure 4. Two bolometers have been used: 1) a closed bolometer and 2) a wire sample. The closed bolometer is made-up of a cylindrical OFHC copper box which encloses the tip of the optical fiber and absorbs totally the optical power delivered by the diode laser. This configuration enables us to characterize the temperature elevation, $T - T_0$ with T_0 ∼4.2 K

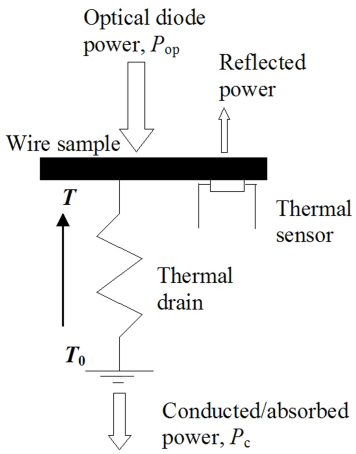

Fig. 4. Schematic drawing of bolometric calibration setup at CNRS/CRTBT.

(at thermal equilibrium), across the thermal drain connecting the bolometer to the heat sink as a function of the DC optical power delivered by the diode laser, $P_{\rm op}$. Then, the copper box was replaced by the wire sample and the same experiment was repeated. As an illustration, Figure 5 shows the thermal response of the two bolometers for a same DC input optical power of $\sim$12 mW. Using the previously-determined thermal drain characteristic, it was possible to evaluate the power, $P_{\rm c}$, conducted away from the sample and the coefficient of optical absorption, ϵ, was estimated as

$$\epsilon = \frac{P_{\rm c}}{P_{\rm op}} \tag{1}$$

The estimation was carried out at various input powers. Figure 6 shows a summary of the results, which yield an average value of $\sim$0.22$\pm$0.07. Finally, the energy absorbed by the sample for a light pulse of duration τ is computed as

$$E_{\rm abs} = \epsilon \int_{\tau} P_{\rm op} dt \quad [\rm J] \tag{2}$$

IV. Experimental Results

Figure 7 shows accumulated voltage traces V_1 for different energy pulses, recorded during a series of measurements at 4.2 K, 7 T and 285 A (85% of $I_{\rm c}$). The pulse duration was set to 30 μs and we gradually increased the current supplied to the diode laser. As the energy pulse is increased, the voltage induced across the heated zone increases until the minimum energy to trigger a quench is reached. Then, the quench propagates and the voltage increases further until it reaches a plateau corresponding to a full transition of the sample section encompassed by V_1.

V. Numerical Model

A. Overview

To analyze our voltage measurements, we simulated the thermo-electric behavior of a Cu/NbTi composite wire undergoing a quench or a recovery. A simplified axi-symmetrical model was developed using Finite Element Method with the

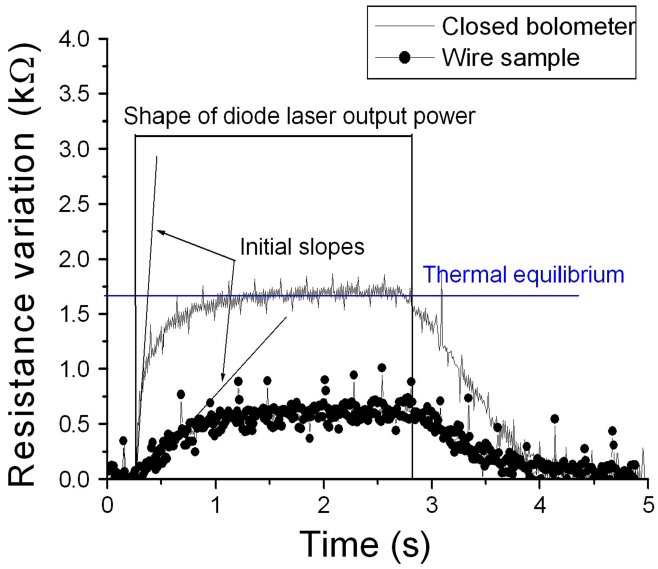

Fig. 5. Time evolution of the resistances of the thermal sensors attached to the bolometers for an input power of $\sim$12 mW: $\Delta R_{\rm TS} = |R_{\rm TS}(T) - R_{\rm TS}(4.2\ K)|$, with $R_{\rm TS}(4.2\ K) \simeq 3000\ \Omega$. (The different initial slopes result from the difference in heat capacities of the two bolometers.)

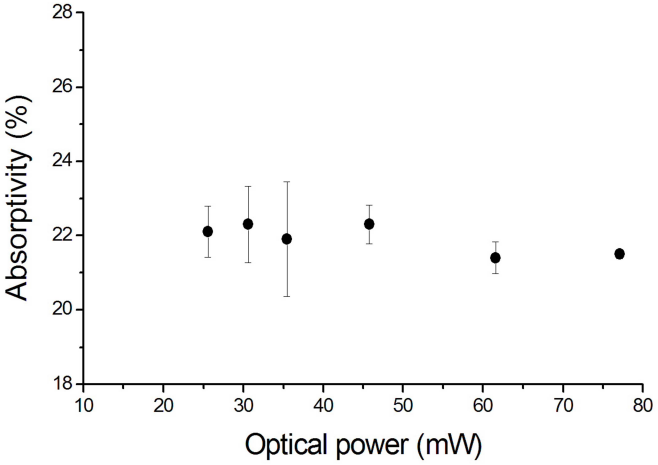

Fig. 6. Absorptivity ($\epsilon\times$100) versus optical power, $P_{\rm op}$, extracted from calibration tests at CNRS/CRTBT.

CASTEM code.

The physical properties being assumed homogeneous over the wire cross-section, the numerical program solves the following non-linear, transient, heat balance equation

$$C_{\rm w}\frac{\partial T}{\partial t} - \frac{\partial}{\partial x}\left[\lambda_{\rm w}\frac{\partial T}{\partial x}\right] - G - Q + H = 0 \tag{3}$$

where

- $C_{\rm w}(T,B)$: average wire heat capacity (J/m^3/K),
- $\lambda_{\rm w}(T,B)$: average wire thermal conductivity (W/m/K),
- $G(T,B)$: heat generation function (W/m^3),
- $Q(t,x)$: initial heat disturbance (W/m^3) [see Fig. 9],
- $H(T,t)$: linearized heat exchanged power (W/m^3).

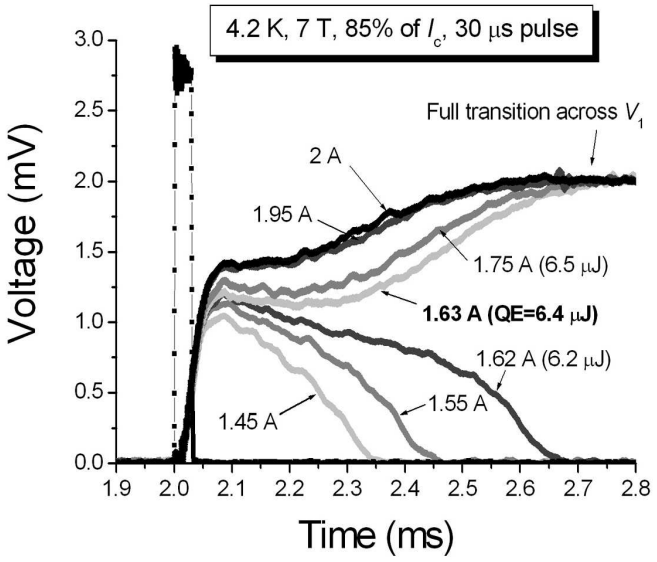

Fig. 7. Transitions and recoveries observed on a 0.82-mm Cu/NbTi multifilament composite wire supplied by Alstom/MSA.

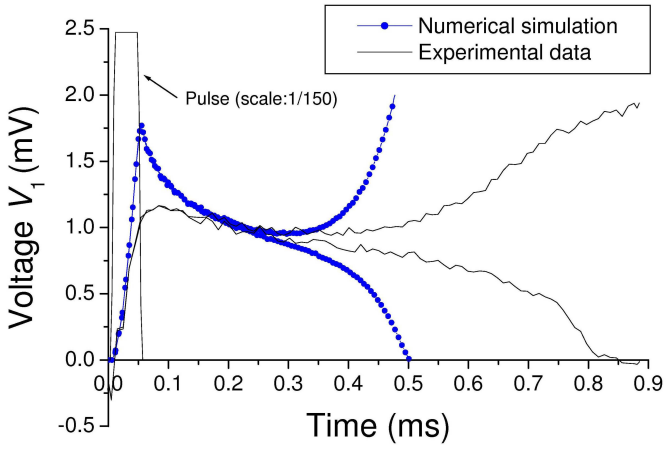

Fig. 8. Comparison between experimental voltage V_1 and numerical simulation for: $a_k = 300$ W/m^2/K^4 and $\eta = 450$ Js^{-6}, and at 4.2 K, 7 T and 85% of I_c.

B. Heat Generation Function

The heat generation function follows the classical linear interpolation [10]

$$G(T,B) = 0, \quad \text{for } T,\ T < T_{cs} \tag{4}$$

$$G(T,B) = G_c \frac{T_{cs} - T}{T_{cs} - T_c}, \quad \text{for } T,\ T_c > T > T_{cs} \tag{5}$$

where

$$G_c(T,B) = \rho_w(T,B) J_w^2 \tag{6}$$

Here, T_{cs} is the current sharing temperature, T_c is the critical temperature, J_w is the current density averaged over the wire cross-section, ρ_w is the average wire resistivity and G_c is the maximum density of dissipated power when all the current flows in the copper matrix.

C. Heat Transfer Function

The heat exchanged power is linearized under the form

$$H(T,t) = \frac{p}{A_w} h (T - T_0) \tag{7}$$

where p is the wetted perimeter, A_w is the wire cross-section and h is the heat-exchange coefficient. To determine h, we rely on Schmidt's model [11].

Two cases are considered depending on the respective values of the energy to form a vapor film, E_f, and the energy transfered from the wire to liquid helium, E_t. E_f can be derived from a simple diffusion model as [10]

$$E_f(t,x) = \eta [t - t_0(x)]^{-0.5} \quad \text{for } t,\ t > t_0 \tag{8}$$

where η is a fitting parameter adjusting the onset time of gaseous helium film, and t_0 is the time at which $T(x)$ exceeds T_{cs}. E_t is computed as

$$E_t(t,x) = \int h[T(x,t)](T - T_0) dt \tag{9}$$

If $E_t < E_f$, we assume a Kapitza-like heat transfer

$$h = a_k (T + T_0)(T^2 + T_0^2) \tag{10}$$

where a_k is a fitting parameter which adjusts the amplitude of heat transfer [11]. Typical values of a_k for copper surface range from 100 W/m^2/K^4 to 1000 W/m^2/K^4 [12].

If $E_t > E_f$, we assume that, as soon as the energy to create the film vapor is exceeded, the liquid helium enters the regime of film vapor

$$h = h_{film} \tag{11}$$

In our computation, we set h_{film} to 250 W/m^2/K.

D. Comparison between Experimental Voltage Traces and Numerical Simulations

Figure 8 compares the results of numerical simulations with experimental voltage traces recorded at 7 T, 4.2 K, 85% of I_c and for a 50 μs pulse. The best agreement between the simulations and the experimental data is obtained with $\eta = 450$ Js$^{-0.6}$ and $a_k = 300$ W/m^2/K^4. The parameter η is the one influencing the most the results while a_k plays only a weak role. The explanation for this can be found in Fig. 9, which compares the time evolution of the heat exchanged flux between wire and coolant with the Joule dissipation normalized to the wetted perimeter (computed at $x = 0$). The decision between quench and recovery clearly takes place while in the vapor film regime where the heat transfer is dominated by conduction and does not depend on a_k any more.

A remarkable feature of Figs. 7 through 9 is the existence of a plateau between the ignition of Joule heating and the quench decision, where there seems to be a metastable thermal equilibrium. This is due to the fact that, for the particular set of operating parameters considered here, we end up in the current sharing zone where only a fraction of G_c is dissipated. For the data of Fig. 9, the metastable equilibrium is reached at $\sim$180 μs where $T \simeq 5.18$ K and $G \simeq 0.4 G_c$. At that time, the normal zone extends over $\sim$6 mm.

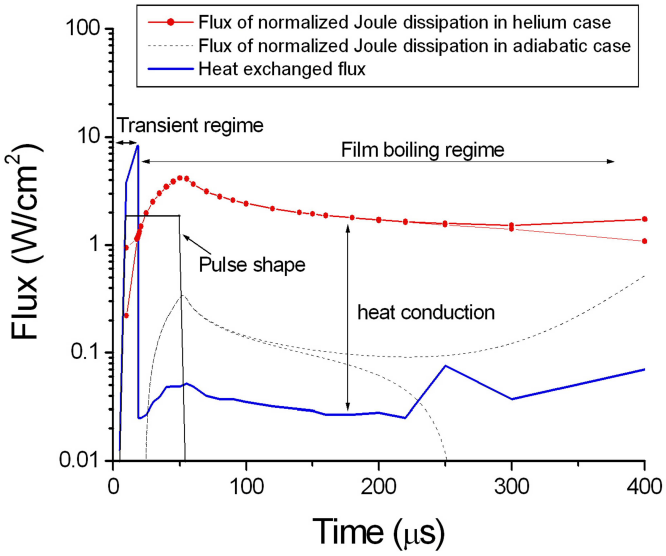

Fig. 9. Comparison of computed heat exchanged flux between sample and helium liquid with Joule dissipation normalized to wetted perimeter at 4.2 K, 7 T, 85% of I_c and for a pulse duration of 50 μs.

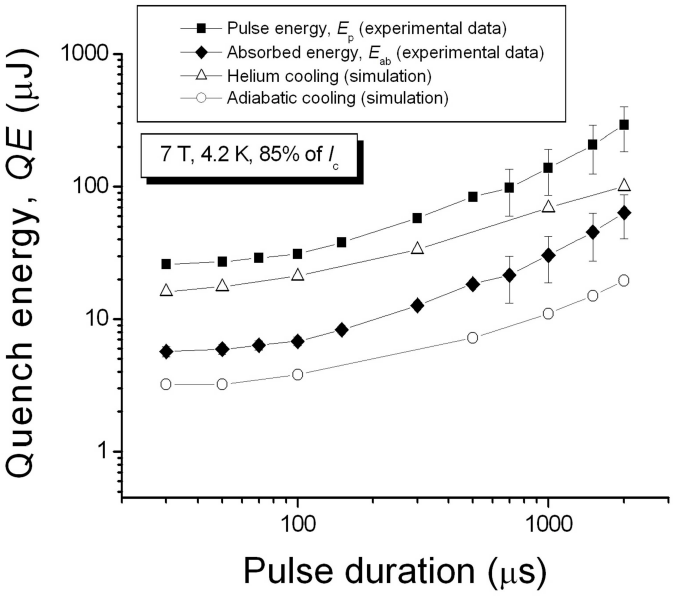

Fig. 10. Pulsed energy and corresponding absorbed energy versus pulse duration at 4.2 K, 7 T and a transport current of 85% of I_c.

E. Minimum Pulse Energy and Estimated Minimum Quench Energy

Figure 10 summarizes the main results on experimental Quench Energies (pulsed energy and corresponding absorbed energy) in comparison to numerical simulations at 4.2 K, 7 T and 85% of I_c. The absorbed energy has been deduced from the pulse energy assuming a coefficient of optical absorption of $\sim$0.22. The numerical simulations with helium cooling yield the right order of magnitude of Minimum Quench Energy. However, the curve lies between the pulse energy and absorbed energy curves. Working the problem backwards, we can use the numerical results to estimate a value of the optical absorption coefficient. From the ratio of computed energy to pulse energy, we get: $\epsilon \simeq 0.6$. The actual value is probably in between. An *in situ* calibration in a vacuum (which we were not able to carry out due to sealing issues in the experimental setup at CEA/Saclay) would be required to draw a final conclusion on this matter.

VI. Conclusion

A better positioning of the sample and the oxidation treatment improved the repeatability of the experiment. Its reproducibility from sample to sample has yet to be demonstrated.

A calibration "proof-test" of the absorption coefficient has been successfully carried out at CNRS/CRTBT. However, it is necessary to perform the calibration *in situ* to achieve a good accuracy.

The experimental results show clear voltage traces which can be interpreted by a simple numerical model. This model, which yields the right order of magnitude of the Minimum Quench Energy, gives some insight into the thermo-electric behavior of composite wires in pool boiling helium I.

Acknowledgment

The authors would like to thank S. Calatroni and M. Malabaila from CERN for their help in oxidizing samples. They would also like to thank T. Dechambre, L. Kulbicki from CEA/Saclay, P. Brosse-Maron, A. Boulbef and G. Barthelemy from CNRS/CRTBT for their precious support, as well as C. Perrier for her assistance.

References

[1] M.N. Wilson and R. Wolf, "Calculation of minimum quench energies in Rutherford-type cables", *IEEE Trans. Appl. Supercond.*, Vol. 7, no. 4, pp. 950-953, 1997.

[2] T. Ogitsu, K. Tsuchiya and A. Devred, "Investigation of wire motion in superconducting magnets", *IEEE Trans. Mag.*, MAG-27, no. 2, pp. 2132-2135, 1991.

[3] K. Seo, M. Morita, S. Nakamura, T. Yamada and Y. Jizo, "Minimum Quench Energy Measurements for Superconducting Wires", *IEEE Trans. Mag.*, Vol. MAG-32, no. 4, pp. 3089-3093, 1996.

[4] D.E. Baynham, D.A. Cragg, D.C. Coombs, P. Bauer and R. Wolf, "Transient Stability of LHC Strands", *IEEE Trans. Appl. Supercond.*, Vol. 9, no. 2, pp. 1109-1112, 1999.

[5] P. Bauer, "Tip heater for Minimum Quench Energy Measurements on Superconducting Strands", *IEEE Trans. Appl. Supercond.*, Vol. 9, no. 2, pp. 1137-1140, 1999.

[6] F. Trillaud, F. Ayela, M. Fratini, D. Leboeuf, and P. Tixador, "Normal Zone generation using a diode laser", *IEEE Trans. Appl. Supercond.*, Vol. 15, no. 2, pp. 3648-3651, 2005.

[7] F. Trillaud, F. Ayela, M. Fratini, D. Leboeuf, and P. Tixador, "A novel technique for minimum quench energy measurements in superconductors using a single mode diode laser", *Cryogenics*, Vol. 45, no. 8, pp. 585-588, 2005.

[8] T.M. Tam, and R.D. Robinson, "Analysis of Factors Controlling Peel Strength of Black Oxide Conversion Coatings", *Plating and Surface Finishing*, pp. 74-77, 1986.

[9] F. Ayela, J.L. Bret, and J. Chaussy, "Absolute magnetometer based on the high frequency modulation of the kinetic inductance of a superconducting thin film", *Journal of Applied Physics*, 78(2), pp. 1334-1341, 1995.

[10] M.N. Wilson, *Superconducting Magnets*, Oxford: Clarendon Press, 1983.

[11] C. Schmidt, "Review of Steady State and Transient Heat Transfer in Pool Boiling Helium I", *International Institute of Refrigeration: Commission A1/2-Saclay*, France, pp. 17-31, 1981.

[12] S. van Sciver, *Helium Cryogenics*, New York: Plenum Press, 1986.